



Research articles

The effects of Fe nano-powders on compaction behaviors and magnetic properties of SMCs



Moosung Choi, Minyeol Kim, Kwiyoung Lee, Junil Song, Jongryoul Kim*

Department of Material Engineering, Hanyang University, Ansan 15588, Republic of Korea

ARTICLE INFO

Keywords:

Soft magnetic composite
Bimodal powder
Tensile strength
Magnetic permeability
Core loss

ABSTRACT

Currently, metallic soft magnetic composites, due to their high saturation magnetization, have attracted much attention for application in high frequency mobile devices. These composites must approach a full densification to achieve the high permeability and magnetic flux density necessary for mobile device applications. This study was carried out to investigate the effects of Fe nano-powders on the compaction behaviors and magnetic properties of Fe-Si alloy composites. Fe-Si micro-powders were fabricated using a gas-atomizer; then, SiO₂ was coated on them to suppress eddy current loss. Fe-nano-powders were obtained using spray-dried Fe₂O₃ powders. These nano-powders were homogeneously mixed with Fe-Si micro-powders to increase the density of the compacts. As a result, the composite with 80 wt% micro-powders showed excellent high frequency properties due to high compaction density. Microstructural analysis shows that changes in the magnetic properties of the composites are dependent on the fill factor and electrical path-ways of non-insulated nano-powders in pores between insulated micro-powders.

1. Introduction

Due to their high magnetic saturation value, good relative permeability, and low magnetic core loss, iron powders have been widely used as a magnetic core material of soft magnetic composites (SMCs). To take full advantage of these excellent properties, full densification of powders should be achieved because the magnetic permeability and magnetic flux density of SMCs are dependent on the SMC density [1]. Due to their high compressibility, pure iron powders with size of several hundred micrometers were reported to reach a compact density of 95% or more via a simple die compaction process [2].

With increasing operation frequency of magnetic devices, there is strong demand to reduce core losses (particularly eddy-current loss) by decreasing the particle size, adding other alloying elements to pure iron, and coating an insulation layer on the powder surface [1]. Unfortunately, achieving high densification using such pre-treated iron powders is very difficult. For example, due to their excellent soft magnetic properties and high electrical resistivity, Fe-Si alloy powders have been widely used as a magnetic core material. However, the addition of Si increases the mechanical strength of the Fe-Si alloy, which severely reduces the compaction density [3,4]. Furthermore, when the average particle size is reduced to less than 20 μm, inter-particle friction and particle bridging become critical problems [5,6]. This indicates that

a simple compaction process is not suitable for the densification of Fe-Si powders applied to high frequency SMCs.

To achieve high densification of hard and fine powders, dynamic compaction methods such as magnetic pulsed consolidation (MPC), or pressure-assisted sintering processes such as hot isostatic pressing (HIP) and spark plasma sintering (SPS), have been widely investigated to increase the compact density [7–11]. These methods include a sintering process, and that is not suitable for the fabrication of SMCs, unlike powders for structural applications or magnetic ferrite powders, which can be sintered. This is because the electrical insulation layer on metal powders can decompose and the metal surface can be exposed during the sintering process [1,2]. Thus, it is required to develop a new method to increase the density of SMCs during the simple compaction process.

It is well known that increasing initial packing density of powders increases the density of compacts. The packing density is dependent on several factors such as particle shape, inter-particle friction, surface chemistry, agglomeration, and size distribution. Among these, the particle size distribution has a strong effect on the packing density [12]. According to previous studies, bimodal powders can increase the packing density by more 10% compared to monomodal powders [13]. Up to now, due to the strong tendency of metal nano-powders to oxidize and aggregate, most studies have focused on micro-sized powders (with or without resin), ceramic powders (magnetic ferrite powders), or

* Corresponding author.

E-mail address: jina@hanyang.ac.kr (J. Kim).

<https://doi.org/10.1016/j.jmmm.2019.02.034>

Received 6 October 2018; Received in revised form 11 February 2019; Accepted 11 February 2019

Available online 12 February 2019

0304-8853/ © 2019 Elsevier B.V. All rights reserved.

simulation [13–17]. Recently, Lee's group demonstrated that a relative compact density of 70% in compacts pressed at 600 MPa could be achieved using structurally-modified agglomerates of pure Fe nano-powders [18,19]. Their results showed that the Fe nano-powders could not aggregate after the reduction process.

According to skin depth calculation result, Fe-Si micro-powder (MP) requires downsizing to tens of micrometers for application of SMCs in the kHz range. In addition, an insulating oxide layer, required to reduce eddy-current loss, should remain after the densification process. Thus, adding pure iron nano-powders (NPs) to hard Fe-Si alloy MPs could be a good method to increase the compact density of SMCs. Improvement of the magnetic properties of SMCs is also expected due to the high saturation magnetization of Fe NPs. Therefore, in this study, a detailed microstructural analysis has been carried out to understand the effects of structurally-modified-agglomerates of pure Fe NPs on the actual packing behavior and frequency dependent magnetic properties of Fe-Si MPs with an SiO₂ insulating layer.

2. Experiments

2.1. Fabrication of single phase nano and micro powders

Commercial α -Fe₂O₃ powders (Kojundo Chemical, 99.9%, ~1 μ m) were used as a starting material for fabricating Fe NPs. To reduce the powder size, bead-milling was carried out using 3 mm steel beads at 2400 rpm for 10 hr. In this process, the volume ratio of powder to balls was kept at 1:8 and methyl alcohol was used as a process control agent. After the bead-milling, the slurry was spray-dried at a pressure of 80 kPa at 30 °C. The spray-dried powders were reduced at 550 °C for 1 h under H₂ atmosphere and kept in a glove box [18,19].

Using a gas atomizer, Fe-3 wt% Si MPs were fabricated under Ar atmosphere. Pure Fe and Si powders were inductively heated to 1650 °C; their melt was then sprayed under an injection pressure of 70 bar. The fabricated powders were sieved through a mesh of under 25 μ m size and annealed at 600 °C for 1 h under H₂ atmosphere. To synthesize the insulation layer over the MPs, they were mixed with 1 wt % magnesium hydroxide and then heat-treated at 900 °C for 6 h under N₂-10% H₂ atmosphere [20]. The fabricated powders were rinsed over ten times with ethanol to remove residual magnesium oxide powders.

2.2. Mixture of Fe nano-powders and Fe-Si micro powders

Spray-dried Fe NPs were observed to be aggregated and weakly sintered during the reduction. These powders must be pulverized and coated to prevent oxidation. In this experiment, stearic acid was used as a coating agent to prevent the NP oxidation, and also as a lubricant for the fabrication of compacts. The 3 mm steel balls, stearic acid, and ethanol were mixed in a vessel and heated to 70 °C to dissolve the stearic acid, after which the vessel was moved to a glove box and Fe NPs were added. Then, to pulverize the aggregated NPs, ball-milling was carried out for 1 h at 60 rpm using a turbula-mixer (Willy A. Bachofen AG, CH-4005). After pulverization, Fe-Si MPs were added and mixed for 5 min in the turbula-mixer (the weight ratio of powder, steel balls, and stearic acid was adjusted to 1:10:0.01). The weight ratio of the Fe-Si MPs was varied from 65 to 100 wt%. The mixed powders were finally dried in an oven at 60 °C for 24 hr.

2.3. Characterization

The microstructures of the powders and their composites were observed using a field emission scanning electron microscope (FE-SEM; Tescan, MIRA3). The particle size and distribution were measured by counting at least 2000 randomly selected particles in the SEM images. The Feret diameter was used to determine the size of the irregularly shaped particles [21]. Cross-sectional images of the Fe-3 wt% Si MPs samples were prepared by focused ion beam (FIB; Tescan, Lyra1)

technique.

The tensile strength (σ_{tensile}) of the composites was evaluated using a diametral compression test [22]. For the test, 1 g sample of mixed powders were compressed into disk shapes having diameter (D) of 10 mm at 800 MPa; then, the thicknesses (h) of the samples were measured. Using a universal testing machine (R&B Inc., UNITECH-T), load (F) was increased until composite was broken in the direction of the plane of disk. The tensile strength was calculated using the following equation.

$$\sigma_{\text{tensile}} = \frac{2F}{\pi Dh} \quad (1)$$

The saturation magnetization (M_s) of powders was analyzed using a vibrating sample magnetometer (VSM; Lakeshore, 7410). To measure the electrical conductivity, permeability, and core loss of composites, the samples were prepared in toroidal shape with inner diameter of 4.5 mm and outer diameter of 8 mm. The electrical conductivity (σ_c) and permeability of composites were measured using, respectively, a four-point probe (AiT, CMT-SR1000N) and an RF impedance/material analyzer (Agilent, E4991A) with a permeability test fixture in the range of 10 MHz – 1 GHz without external DC magnetic field. Using a BH analyzer (Iwatsu, SY-8219), the core loss (P_c) was measured at a constant magnetic flux density of 100 mT in the range of 1–100 kHz. The measured P_c was divided into the hysteresis loss (P_h) and the eddy current loss (P_e); P_e included both classical and anomalous eddy losses. Assuming that both classical and anomalous eddy losses are proportional to the square of the frequency, the relationship between P_h , P_e , and P_c , measured at frequency of f , can be simply expressed as,

$$P_c = P_h + P_e = f \cdot P_{h,1\text{Hz}} + f^2 \cdot P_{e,1\text{Hz}} \quad (2)$$

where $P_{h,1\text{Hz}}$ and $P_{e,1\text{Hz}}$ are P_h and P_e , respectively, measured at 1 Hz.

3. Results and discussion

3.1. Powder characteristics

Fig. 1(a) provides an SEM image of the spray-dried Fe₂O₃ nano-powder agglomerates. As can be seen in the figure, the agglomerates have spherical shape with a size distribution of 1–5 μ m. On the other hand, the enlarged SEM image shown in Fig. 1(b) indicates that the Fe₂O₃ NPs have irregular shapes with sizes of 20–50 nm. After reducing the samples at 550 °C, SEM images of the Fe NP agglomerates were obtained and presented in Fig. 1(c) and (d). As shown in Fig. 1(c), most of agglomerates still possess a spherical shape, although some agglomerates have disintegrated. These reduced agglomerates were confirmed by XRD (Fig. 2, JCPDS file no. 71-4409) and VSM (Fig. 3, 212.6 emu/g of M_s) to have a single iron phase. The enlarged SEM image of the Fe agglomerates (Fig. 1(d)) shows that the reduced Fe NPs had a bimodal type size distribution of 325 ± 22 nm and 28 ± 3 nm. This bimodal growth of NPs is due to the different thermodynamic and kinetic conditions of NPs with non-uniform packing structure in the spray-dried agglomerate [19]. Thus, some NPs in the agglomerates is coarsened and weakly sintered during the reduction process. It is also noted that the agglomerates themselves were not sintered or coarsened after the reduction process, as shown in the Fig. 1(c). This clearly shows that the coarsening and sintering of the NPs occurred only inside the spray-dried agglomerates during the reduction process. Furthermore, due to the lack of apparent interconnection between them, the sintered NPs are expected to be easily separated even at low ball-mill energy.

SEM images of fabricated Fe-3 wt%Si MPs are provided in Fig. 4(a) and (b). As can be seen, the powders have spherical shapes, and their surfaces were smooth and clean enough to see the internal grains. These MPs had a mean size (D_{50}) of 7 μ m with a Gaussian size distribution from 1 to 25 μ m. The XRD pattern of the powders shown a single iron phase (Fig. 2) and their saturation magnetization reached 210.6 emu/g (Fig. 3). To avoid eddy current loss between particles, the MPs were

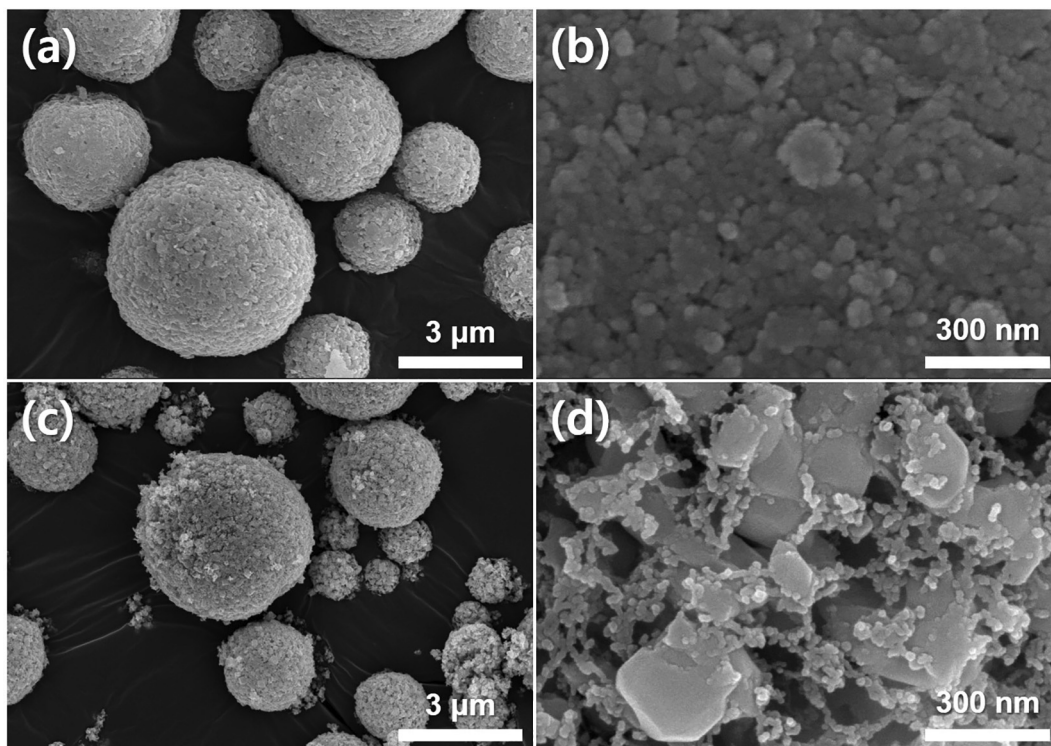


Fig. 1. SEM and enlarged images of (a), (b) Fe_2O_3 nano-powder agglomerates and (c), (d) reduced Fe nano-powders agglomerates.

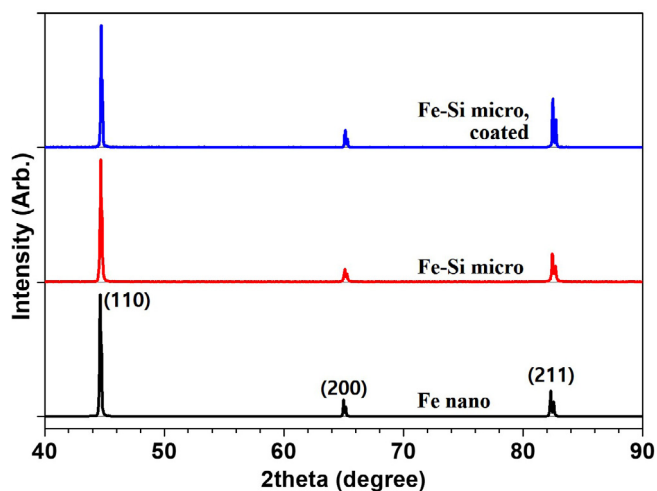


Fig. 2. XRD patterns of Fe nano-powders, Fe-Si micro-powders, and coated Fe-Si micro-powders.

heat-treated at $900\text{ }^\circ\text{C}$ for 6 hr with magnesium hydroxide to form surface insulation layers. Fig. 4(c) shows that, except for having fine particles on the surface, the morphology of the Fe-Si MP is similar to that of the as-coated Fe-Si MP shown in Fig. 4(b). On contrary, the energy dispersive spectrum (EDS) results (tables in Fig. 4(b) and (c)) clearly showed increases in the Si and O peak intensities on the whole surface area. Furthermore, the fine particles have an Mg K peak, indicating that they could be Mg-Si-oxides. To confirm the micro-structural development, a cross-sectional image of the MPs prepared by FIB was obtained and is shown in Fig. 4(d). As can be seen in the figure, the oxide layer was well formed around the MP. The thickness of the oxide layer was measured in the range of 20–500 nm. These results clearly prove that Si oxide layers were successfully formed on the surfaces of the MPs.

As can be seen in Fig. 3, the saturation magnetization of the MPs

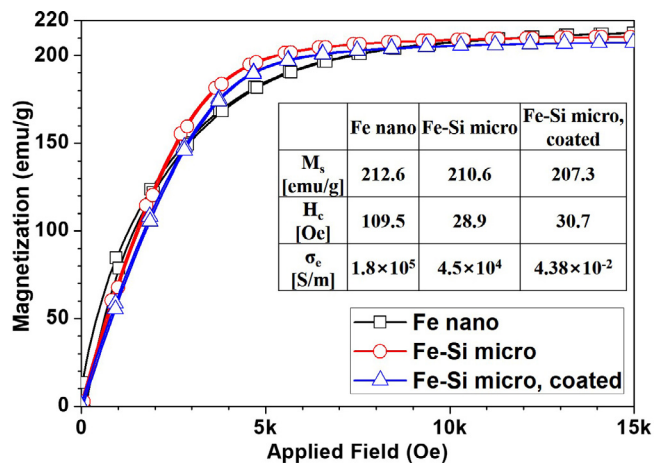


Fig. 3. VSM results of Fe nano-powders, Fe-Si micro-powders, and coated Fe-Si micro-powders. Electrical conductivities (σ_c) of the powder compacts are also indicated.

decreased slightly from 210.6 to 207.3 emu/g after the surface oxidation process. Assuming that the oxide layer is SiO_2 , the weight fraction of the coated layer is only about 1.6 wt%. Nevertheless, the conductivity after the compaction of powders significantly decreased from 4.5×10^4 S/m (non-coated Fe-Si powders) to 4.38×10^{-2} S/m (coated powders), a change of about 10^6 times. According to a simulation study on eddy-current loss of powder cores, to suppress eddy current loss between Fe-based-MPs, the conductivity of insulated powders should be 10^5 times smaller than that of non-insulated powders [23]. Thus, the conductivity drop in this study is sufficient to suppress the eddy current loss. Consequently, the results of magnetization and conductivity analyses demonstrate that the coating layer of Fe-Si powders is thin enough to maintain saturation magnetization but sufficiently thick to suppress eddy current loss.

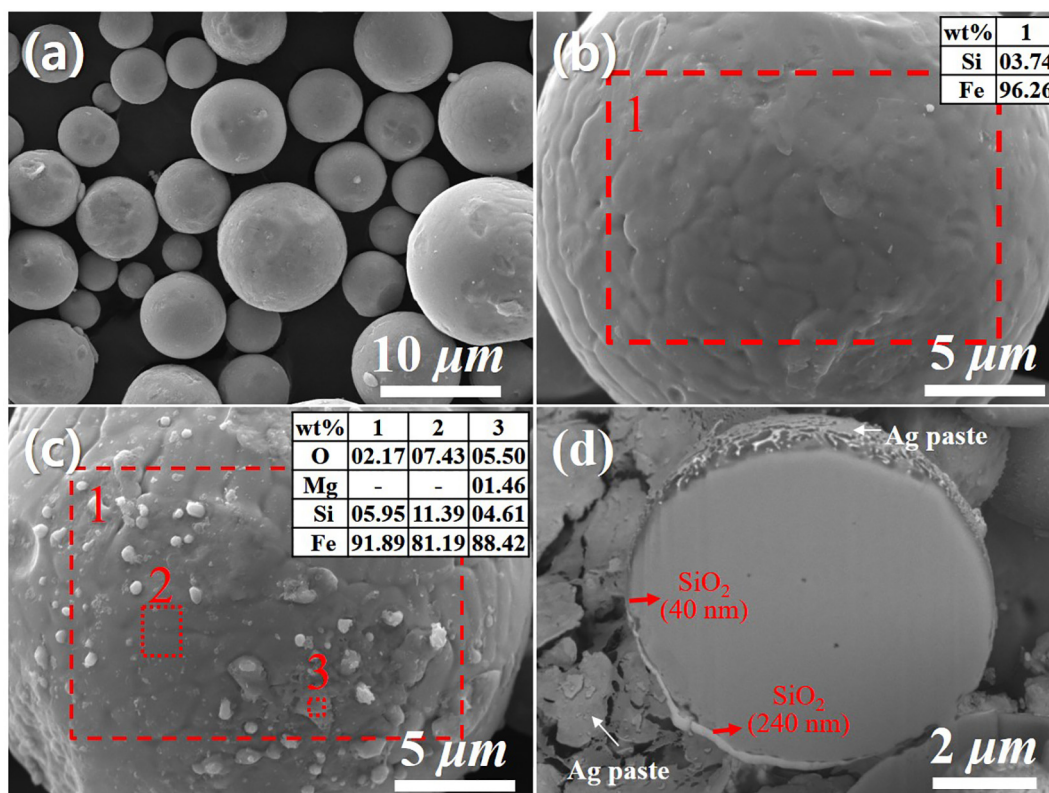


Fig. 4. SEM image of (a), (b) as-coated Fe-Si micro-powders, (c) coated micro-powder, and (d) cross-sectional image of coated micro-powder.

3.2. Compaction behaviors

Table 1 shows the changes in density, electrical conductivity, and tensile strength in composites compressed at 800 MPa as a function of Fe NP contents. As shown in the table, the density of the composite containing only MPs (0 wt% NPs) was measured at 6.03 g/cm³, which is 78.82% of the Fe-3 wt% Si theoretical density (TD, 7.65 g/cm³). In the general process of metal powder compaction, it is considered that metal powders are first rearranged and then plastic-deformed to increase the density of compacts [24]. Meanwhile, as shown in Fig. 5(a), it was found that Fe-Si powders rarely deformed even at a high compaction pressure of 800 MPa due to their high strength [3,4]. Furthermore, the composite containing 0 wt% NPs was too brittle to maintain the shape of composite because the composite has many pores (marked with circles) as shown in Fig. 5(a).

In order to understand this result, the tensile strength of the composites was measured by diametral compression test and results are presented in Table 1. The tensile strengths of the composites can denote the frictional force between powders. As shown in the table, the tensile

Table 1

Changes in density, electrical conductivity, and tensile strength of composites as function of Fe nano-powder content.

Composites [wt% NPs]	Density [g/cm ³]	Electrical conductivity [S/m]	Tensile strength [MPa]
0	6.03	0.044	0.44
5	6.31	1.52	1.71
10	6.44	5.86	6.31
15	6.53	83.6	8.28
20	6.62	190.7	9.73
25	6.59	793.5	17.17
30	6.55	1007	23.74
35	6.46	1953	31.34
100	5.71	179,530	277.1

strength of the composite of 0 wt% NPs is 0.44 MPa. This low composite strength indicates that the frictional force between the MPs is too low to maintain the composite. The frictional force of powders is dependent on the inter-particle contact area, specific surface area, and powder shapes [24]. Thus, the powders should be accompanied a complete plastic-deformation step, or should have another substance added to increase the frictional force. Due to their large specific surface areas, NPs can be effective substances to increase the frictional force. In addition, the irregular shapes of the NPs in this study can increase the frictional force. As expected, the tensile strength of the composites increases with increasing NP content, as shown in Table 1. In addition, the composite containing 10 wt% NPs or more did not exhibit any fractures during the ejection process.

To increase the density of the composite, one effective method is to fill the pores between the MPs with NPs. To realize this process, NPs have to be well separated from one another and dispersed among MPs. In addition, NPs should not destroy the skeleton of the MPs, but only fill up pores between MPs. Fig. 5(a)–(e) shows microstructural changes in Fe-Si composites with increasing content of pure Fe NPs. As the NP content increases, the pores between MPs began to fill up by the NPs. Until adding of 15 wt% NPs, some of pores were still not filled; see circles in Fig. 5(b)–(d). The NPs fully filled the pores up at 20 wt% NPs without destroying the skeleton of MPs as shown in Fig. 5(e). As a result, the density of compacts increased from 6.03 to 6.62 g/cm³ (86.54%TD) at the composite of 20 wt% NPs. This increase in the density is caused by the multi-modal mixing of NPs and MPs [13].

As shown in Fig. 5(f)–(h), further increases of NPs to over 20 wt% pushed out the MPs and resulted in locally separated NP areas (marked with dotted circles in the figures) in the composite. As the NP content increases more than the maximum density condition (20 wt% in this study), the locally separated NP areas should be increased. This behavior results in a decrease in the density of composite [13]. It is well observed in this study as shown in the figure and Table 1. Moreover, this massive interconnection between NPs can account for the sharp

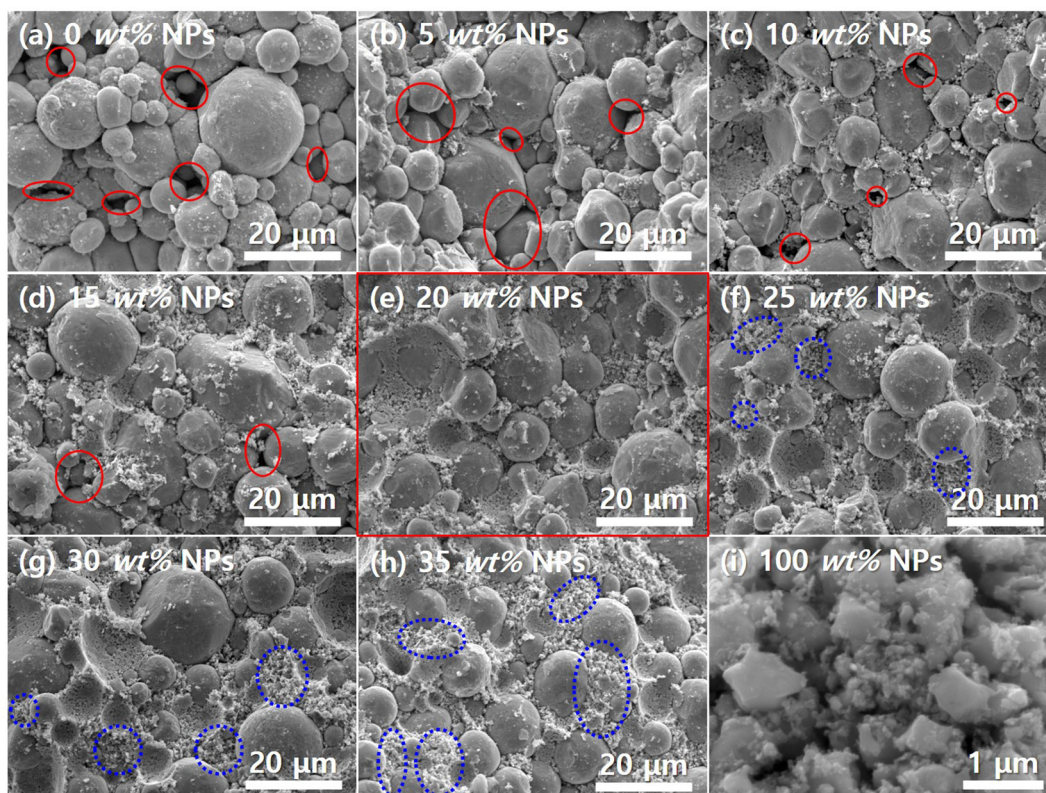


Fig. 5. SEM images of fractured surface of composites; weight fraction of Fe nano-powders was controlled from 0 wt% to 100 wt%.

increases in electrical conductivity and tensile strength. Finally, the density of composite containing only NPs dropped to 5.71 g/cm^3 as can be seen in Table 1; Fig. 5(e) shows the morphology of the composite. The decrease in the density is because that the frictional force of the NPs is so large as to make it very difficult to rearrange them during compaction compared to the MPs. These morphological developments with the addition of NPs are in good agreement with the changes in density, conductivity and tensile strength shown in Table 1.

3.3. Magnetic properties

Fig. 6 shows changes in the relative permeability of composites as a function of Fe NP contents. As can be seen in the figure, the real permeability (μ') at 1 MHz increases from 28 to 38 as the NP content increases to 20 wt% (the maximum density condition) and then decreases to 14. This dependence of permeability on the NP content is in good accordance with the density change of the composites. Thus, it is considered that the high initial real permeability is caused by the increase of the magnetic flux density under the same external magnetic field as the density increases. Unlike the behavior of initial real permeability, the frequency where imaginary permeability (μ'') has a maximum value continuously decreases as the content of NPs increases. This indicates that the magnetic loss behaviors are not dependent on the density change of the composite.

In order to clarify the loss behaviors of the composites, the magnetic loss tangent ($\tan\delta_m = \mu''/\mu'$) are presented in Fig. 7. In the figure, the yellow stars denote the maximum μ'' frequency of each composite. It should be also noted that the maximum μ'' frequency can shift to lower frequencies due to the increase of eddy current loss [25,26]. Up to the addition of 10 wt% NPs, the $\tan\delta_m$ values of these composites were almost null at below 10 MHz; then, the abrupt increase of $\tan\delta_m$ occurred at several hundred MHz. This change in the slope of $\tan\delta_m$ indicates that the loss mechanism changes from eddy current loss to resonance loss with increasing frequency. In addition, with increasing amounts of NPs,

the frequencies at maximum μ'' were almost unchanged and a noticeable increase in $\tan\delta_m$ values were observed above the maximum μ'' frequency. These results indicate that, up to the addition of 10 wt% NPs, additional eddy current losses induced from NPs occurred only at very high frequencies and did not have a significantly effect on the magnetic loss behavior of composite. On the contrary, a further increase of the NP content up to 20 wt% NPs began to affect the magnetic loss behavior of composite. As NP content increases, the maximum μ'' frequency decreased to under 100 MHz and $\tan\delta_m$ values in the range of few MHz to 100 MHz increased. In particular, composites with more than 25 wt% NPs exhibited completely different $\tan\delta_m$ behaviors compared to composites with less than 20 wt% NPs. In composites with high NP concentration, the maximum μ'' frequencies sharply decreased and $\tan\delta_m$ value began to appear at 1 MHz. A composite containing only NPs shown a high $\tan\delta_m$ value at 1 MHz. Furthermore, the $\tan\delta_m$ slopes of these composite above 25 wt% NPs were almost linear up to 1 GHz. Even in the composite of 100 wt% NPs, the abrupt increase in $\tan\delta_m$ value was not observed. These results indicate that the losses of composites with high NP concentration were dominated by eddy current loss. Thus, when the NP content increased to more than 10 wt%, the magnetic loss behavior began to be dominated by eddy current loss. This behavior resulted in decreasing the maximum μ'' frequency.

These results strongly indicate that the magnetic loss behaviors are closely related to the electrical conductivity changes instead of the density changed of the composites as shown in Table 1. Namely, the losses are highly related to the microstructure. As shown in Fig. 5, NPs initially occupy pores between insulated MPs. When the NP content is over 20 wt%, the NPs push out the MPs and begin to make large clusters. Because these NPs have no insulating layer and have high surface area, an abrupt increase of the electrical conductivity occurs when the NP content is over 20 wt% NPs. Thus, this microstructural change can qualitatively show that the loss mechanism of composites sharply changes when the NP content increases from 20 to 25 wt%.

As discussed previously, because non-insulated NPs are effectively

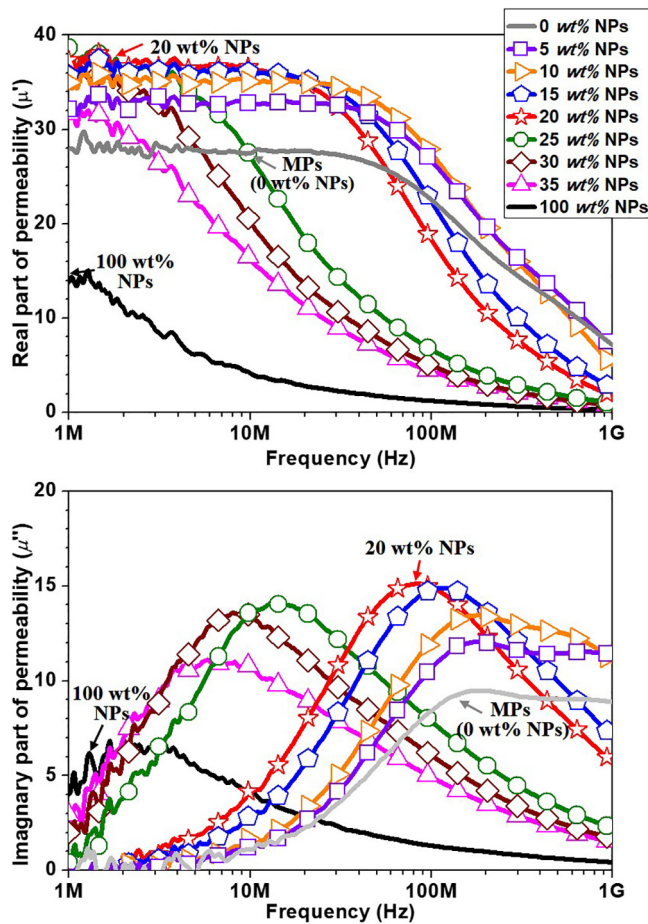


Fig. 6. Changes in the relative permeability of composites as a function of Fe nano-powder content.

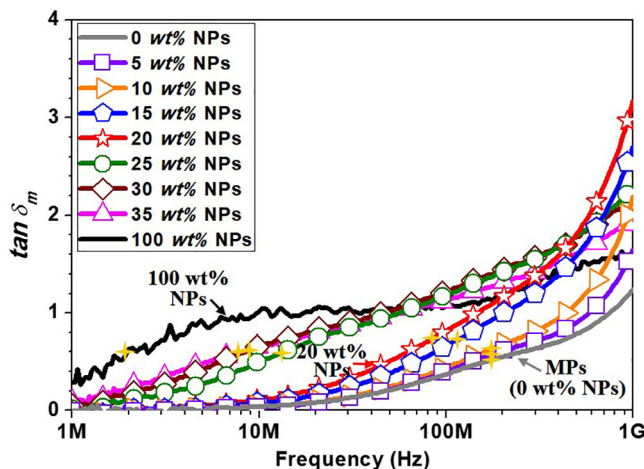


Fig. 7. Changes in the loss tangent ($\tan \delta_m$) of composites as a function of Fe nano-powder content.

trapped between insulated MPs without noticeable increase of electrical conductivity, adding a certain amount of pure Fe NPs (20 wt% in this study) to the coated Fe-Si MP composites is an effective way to control the high frequency magnetic properties of metal cores by changing the microstructures. Furthermore, the composites can increase the magnetic flux density due to the increase of the composite density. Thus, to understand the change of the soft magnetic properties, it is necessary to investigate the core losses of composites.

Table 2 shows changes in the core loss (P_c) of the composites as the

Table 2

Change in the core loss (P_c) of composites as function of Fe nano-powder content.

wt% NPs	P_c [W/kg]	P_h [W/kg]	P_e [W/kg]
0	380.3	371.7	8.5
5	346	337.4	8.6
10	312	302.7	9.3
15	283.7	272.9	10.8
20	286.1	272.2	13.9
25	318.8	291.7	27.1
30	353.3	319.5	33.8
35	385.7	325.8	59.9
100	6474	1253	5221

Fe NP content changes. The P_c was measured at 100 kHz and under a constant magnetic flux density of 100 mT. The hysteresis (P_h) and eddy-current loss (P_e), calculated from the P_c , are also shown in the table. As can be seen in the table, P_e continuously increase with increasing NP content, but account for less than 5% of P_c until 20 wt% NPs. As discussed in section 3.1, the conductivity of insulated MPs is 10^6 times smaller than that of non-insulated MPs. Thus, the eddy current loss of the composite without NPs is induced by the inner area of the insulated MPs. This indicates that the increment of P_e in composites containing NPs are caused by the NPs. Thus, additional eddy-current loss induced by Fe NPs is effectively suppressed up to an NP content of 20 wt%, indicating that NPs can be trapped in the voids of MPs.

On the other hand, P_h of the composite dropped from 371.7 W/kg to 272.2 W/kg as the NP content increases from 0 to 20 wt% NPs. This dependence of p_h on the NP content can be explained by the changes in the permeability shown in Fig. 6 because an increase in permeability generally causes a decrease of hysteresis loss. When the NP content increased to more than 20 wt% NPs, P_h deteriorated again. As an example, the P_h of the composite containing 30 wt% NPs (P_h , 319.5 W/kg) is larger than that of the composite with 15 wt% NPs (P_h , 272.9 W/kg), although the density values of these composites are similar at 6.55 and 6.53 g/cm³, respectively. To understand this discrepancy, the coercivity of the NPs (109.5 Oe) and MPs (30.7 Oe), shown in Fig. 3, should be noted. This indicates that the NPs can contribute to the increase of p_h as the NP content increases. Up to 20 wt% NPs, this contribution is less than the decrement of p_h due to increasing of the composite density. Therefore, to obtain excellent soft magnetic properties of the composites, it is critical to confine the NPs to voids between MPs.

4. Conclusion

In order to enhance the high frequency properties of metal micro-powder composites, Fe NP agglomerates and SiO₂ layer coated Fe-Si MPs were prepared and mixed homogeneously. These bimodal powders were compressed at 800 MPa to make composites. Despite the low compressibility of Fe-Si MPs, the high frictional forces of the NPs could increase the tensile strength of the composites. Changes in the magnetic properties and microstructure of these Fe-Si composites were investigated with increasing Fe NP content.

Microstructural analysis of the composites showed that the NPs initially occupied voids between MPs; interconnection networks of NPs across among MPs began to form when the NP content reached 20 wt%. Due to these morphological developments, the density reached a maximum at an NP content of 20 wt%. Furthermore, the initial real permeability and P_h also reached maximum and minimum values, respectively, at 20 wt%. The electrical conductivity of the composites continuously increased with increasing NP content; however, the eddy current loss under 1 MHz was well suppressed up to 20 wt% NP.

Consequently, composites composed of bimodal powders were confirmed as an effective way to increase the tensile strength, high frequency characteristics, and soft magnetic properties as long as NPs

remained in the voids between MPs.

Acknowledgements

This work was supported by the Human Resources Development program (No. 20174030201830) of the Korea Institute of Energy Technology Evaluation and Planning (KETEP) grant funded by the Korea government Ministry of Trade, Industry and Energy, Republic of Korea; and Future Materials Discovery Program through the National Research Foundation of Korea (NRF) funded by the Ministry of Science, ICT & Future Planning (NRF-2016M3D1A1027836), Republic of Korea.

References

- [1] H. Shokrollahi, K. Janghorban, Soft magnetic composite materials (SMCs), *J. Mater. Process. Technol.* 189 (2007) 1–12.
- [2] S. Lee, M. Choi, J. Kim, Magnetic properties of pure iron soft magnetic composites coated by manganese phosphates, *IEEE Trans. Magn.* (2017).
- [3] B.D. Cullity, C.D. Graham, *Introduction to Magnetic Materials*, John Wiley & Sons, 2011.
- [4] T. Saito, H. Tsuruta, A. Watanabe, T. Ishimine, T. Ueno, Pure-iron/iron-based-alloy hybrid soft magnetic powder cores compacted at ultra-high pressure, *AIP Adv.* 8 (2018) 047708.
- [5] R. Wakeman, Packing densities of particles with log-normal size distributions, *Powder Technol.* 11 (1975) 297–299.
- [6] J. Visser, Van der Waals and other cohesive forces affecting powder fluidization, *Powder Technol.* 58 (1989) 1–10.
- [7] S. Hong, G. Lee, C. Rhee, W. Kim, K. Lee, Magnetic pulsed compaction of ferromagnetic nano-powders for soft-magnetic core, *Mater. Sci. Eng., A* 449 (2007) 401–406.
- [8] Z.A. Munir, U. Anselmi-Tamburini, M. Ohyanagi, The effect of electric field and pressure on the synthesis and consolidation of materials: a review of the spark plasma sintering method, *J. Mater. Sci.* 41 (2006) 763–777.
- [9] O. Guillon, J. Gonzalez-Julian, B. Dargatz, T. Kessel, G. Schierning, J. Räthel, M. Herrmann, Field-assisted sintering technology/spark plasma sintering: mechanisms, materials, and technology developments, *Adv. Eng. Mater.* 16 (2014) 830–849.
- [10] M. Yu, S. Grasso, R. Mckinnon, T. Saunders, M.J. Reece, Review of flash sintering: materials, mechanisms and modelling, *Adv. Appl. Ceram.* 116 (2017) 24–60.
- [11] B. AlMangour, D. Grzesiak, J.-M. Yang, Selective laser melting of TiB₂/316L stainless steel composites: The roles of powder preparation and hot isostatic pressing post-treatment, *Powder Technol.* 309 (2017) 37–48.
- [12] R. German, *Particle Packing Characteristics*, 135–159; 1989, Princeton, New Jersey, MPIF, 1989.
- [13] R. McGeary, Mechanical packing of spherical particles, *J. Am. Ceram. Soc.* 44 (1961) 513–522.
- [14] R.D. Groot, S.D. Stoyanov, Close packing density and fracture strength of adsorbed polydisperse particle layers, *Soft Matter* 7 (2011) 4750–4761.
- [15] V. Wong, A.K.H. Kwan, A 3-parameter model for packing density prediction of ternary mixes of spherical particles, *Powder Technol.* 268 (2014) 357–367.
- [16] B. Ma, J. Herchenroeder, B. Smith, M. Suda, D. Brown, Z. Chen, Recent development in bonded NdFeB magnets, *J. Magn. Magn. Mater.* 239 (2002) 418–423.
- [17] R. Malik, S. Annapoorni, S. Lamba, V.R. Reddy, A. Gupta, P. Sharma, A. Inoue, Mössbauer and magnetic studies in nickel ferrite nanoparticles: effect of size distribution, *J. Magn. Magn. Mater.* 322 (2010) 3742–3747.
- [18] G.-Y. Lee, J.-L. Song, J.-S. Lee, Reaction kinetics and phase transformation during hydrogen reduction of spherical Fe₂O₃ nanopowder agglomerates, *Powder Technol.* 302 (2016) 215–221.
- [19] J.-L. Song, G.-Y. Lee, J.-P. Choi, J.-S. Lee, Compaction behavior of bimodal iron nanopowder agglomerate, *Powder Technol.* 338 (2018) 333–341.
- [20] K. Lee, M. Choi, J. Kim, High-frequency properties of Fe-4.5 wt% Si powders with an insulating layer synthesized by a modified dew point treatment, *IEEE Trans. Magn.* (2017).
- [21] T. Allen, *Particle Size Measurement*, Springer, 2013.
- [22] J. Amorós, V. Cantavella, J. Jarque, C. Felfu, Green strength testing of pressed compacts: an analysis of the different methods, *J. Eur. Ceram. Soc.* 28 (2008) 701–710.
- [23] P. Jang, B. Lee, Effects of insulator resistivity on eddy current loss of compressed powder cores studied by FEM, *IEEE Trans. Magn.* 45 (2009) 2781–2783.
- [24] R.M. German, *Powder, metallurgy and particulate materials processing: the processes, materials, products, properties, and applications*, Metal powder industries federation, Princeton (2005).
- [25] R. Ramprasad, P. Zurcher, M. Petras, M. Miller, P. Renaud, Magnetic properties of metallic ferromagnetic nanoparticle composites, *J. Appl. Phys.* 96 (2004) 519–529.
- [26] M. Choi, S. Lee, J. Kim, Clustering effect on the frequency-dependent magnetic properties of Fe-Co micro hollow fiber composites, *IEEE Trans. Magn.* (2017).